JOURNAL OF MATERIALS SCIENCE 28 (1993) 5349–5354

The morphology of particles of minor phases in a commercial Al–7.12 wt% Si alloy

C.C. CHAMA
Department of Metallurgy and Mineral Processing, University of Zambia, PO Box 32379, 10101 Lusaka, Zambia

The morphology of particles of minor phases was monitored in an Al–7.12 wt % Si alloy in three different states: as-cast, hot isostatically pressed (HIPed) and heat-treated. In all of these states, the minor phases existing in this alloy were secondary silicon-rich particles and those which are iron-containing–$Al_{12}Fe_3Si$ and ($FeAl_6$) Si. The major phase was primary silicon-rich particles. The HIPed and heat-treated materials contained an additional phase, the iron-containing particles $Al_9Fe_2Si_2$. It was found that secondary silicon-rich particles in the as-cast material were plate-like, spherical or fibrous. On the other hand, the few iron-containing particles in the as-cast material were needle-like. During HIPing or heat treatment, the iron-containing particles which precipitated also had a needle-like morphology. Most of the non-spherical secondary silicon-rich particles tended to spheroidize during HIPing or heat treatment. Fibrous secondary silicon-rich particles were not present in the HIPed or heat-treated materials.

Nomenclature

f	Shape factor
ΔG^*_{het}	Activation energy barrier for heterogeneous nucleation
ΔG^*_{hu}	Activation energy barrier for homogeneous nucleation
ΔG_V	Volume free energy change
r^*	Critical nucleus size
$\gamma_{\alpha\beta}$	Interfacial energy

1. Introduction

The morphology of particles in materials is usually of considerable interest as it assists in explaining some features of microstructural development. The formation of particles with specific morphologies is by the classical nucleation and growth mechanisms. Some of the more common particle morphologies that have been found in many microstructures are spheres, rods, lamellae and plates. In certain instances, combinations of morphologies, such as a cylindrical particle with spherical tips, exist. The morphology that a particular particle will adopt under existing phase transformation conditions can be predicted by utilizing its interfacial energy in the γ-plot and Wulff construction [1]. The two main parameters which can be used to determine whether a particular morphology should form are critical particle size and the activation energy. For a spherical β particle nucleating in an α matrix, such as that in Fig. 1a, the critical nucleus size and activation energy are

$$r^* = -\frac{2\gamma_{\alpha\beta}}{\Delta G_v} \quad (1)$$

$$\Delta G^*_{hu} = \frac{16\pi\gamma^3_{\alpha\beta}}{3\Delta G^2_v} \quad (2)$$

Equations 1 and 2 apply to an unfaceted spherical nucleus under homogeneous nucleation conditions. In most phase transformation processes, the energy barrier to nucleation (ΔG^*_{hu}) is minimized by the interfacial energy ($\gamma_{\alpha\beta}$) acquiring low values. This requirement of minimum interfacial energy makes spherical morphologies ideal according to considerations of the γ-plot and Wulff construction. One of the major ways by which a non-spherical particle can minimize its interfacial energy is by transforming to a morphology which is partially or completely spherical. This transformation to a spherical morphology is particularly significant when materials are exposed to elevated temperatures [2]. Spheroidization can proceed in two ways: the parent particle can transform either to a single sphere of the same volume or to several spheres [3]. Apart from spherical morphologies, there is evidence for the existence in some aluminium-base alloys of particles with intricate morphologies [4, 5].

Usually, nucleation is heterogeneous and occurs predominantly at grain boundaries, dislocations and vacancy clusters. For non-spherical particles forming heterogeneously, the activation energy can be expressed as

$$\Delta G^*_{het} = \Delta G^*_{hu} f \quad (3)$$

In the case of heterogeneous nucleation of non-spherical particles, $f < 1$. Since ΔG^*_{het} is less than ΔG^*_{hu}, heterogeneous nucleation would be favoured over homogeneous nucleation because of the lower energy required for this transformation to proceed. In addi-

0022–2461 © *1993 Chapman & Hall*

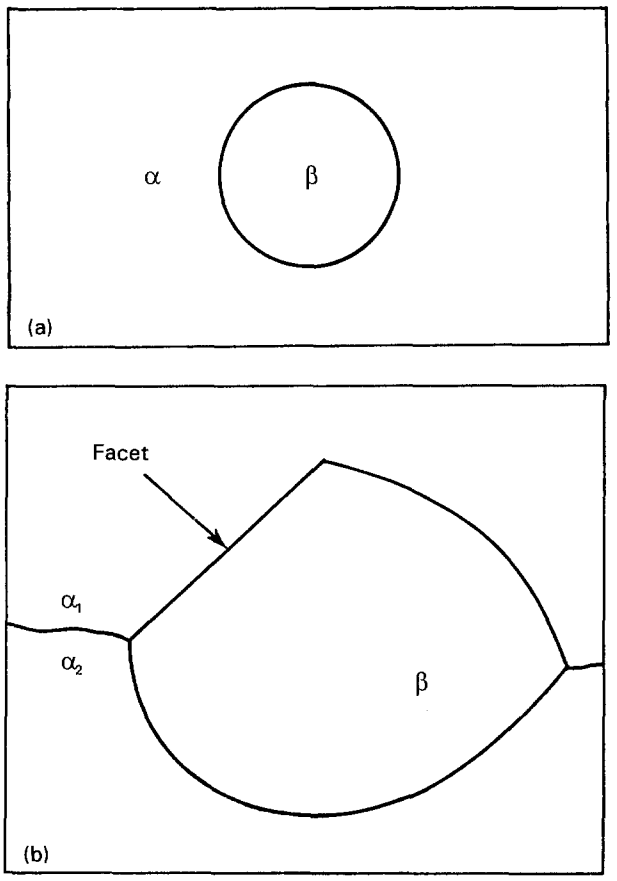

Figure 1 Geometry of (a) spherical and (b) faceted particles.

tion to spheroidization, the interfacial energy can also be minimized by a precipitate adopting facets [6, 7] as shown in Fig. 1b for a β particle at an α_1–α_2 grain boundary. Several different geometries of facets are possible [8]. After heat treatment, it has been observed that most silicon particles become faceted [9]. These facets exist on the {1 0 0} and {1 1 1} surfaces of silicon particles [10, 11]. Furthermore, facets on {2 1 1} surfaces of silicon have also been observed [12]. For cubic materials such as silicon, it is expected that facets will be formed on surfaces such as {1 0 0} and {1 1 1} since these have the lowest free energies. Other particles, such as Mg_2Si [13] and those which are iron-containing like Al_7Cu_2Fe [14], show a variety of morphologies.

2. Experimental procedure

Microstructural investigations were conducted on the casting of composition given in Table I when in the as-cast state or after HIPing at 68.95 MPa and various combinations of time (15–120 min) and temperature (500–560 °C). HIPing was performed on this casting in order to eliminate porosity. In addition, microstructures of materials which had been subjected to the following heat-treatment process were investigated: anneal 30 min at 510 °C → water-quench → age 1 or 48 h at 204 °C.

Specimens for scanning electron microscopy (SEM) were electropolished at 5 V for about 30 s in the solution given in Table II. Afterwards, the specimens were examined in an ISI Super IIIA SEM operating at 10 or 15 kV. Foils for transmission electron microscopy (TEM) were jet-polished at 5 V by using the solution in Table III. An EM 420T microscope operating at 120 kV was thereafter used for TEM investigations.

3. Results and discussion

3.1. As-cast material

Upon solidification, this alloy has the microstructure shown in Fig. 2. Two types of precipitate are present within the aluminium-rich matrix: large or primary (A in Fig. 2) and very small or secondary (around region B) silicon-rich particles. This article focuses on the morphology of particles with a size such as those around region B in Fig. 2 and others which are smaller. A TEM dark-field image of a fibrous secondary silicon-rich particle is shown in Fig. 3. This secondary silicon-rich particle (A) has several fibres (B, C, D and E) with an interfibre spacing of about 200 nm. The tips of some of these fibres, such as E, are partially spheroidized. This is to be expected, since the morphology of most precipitate particles can sometimes involve a combination of more than one shape due to instabilities that may be encountered during phase transformation. One of the morphologies that will exist in

TABLE I Composition of the casting (wt %)

Si	Cu	Mg	Fe	Sb	Al
7.12	0.05	0.16	0.29	0.06	Balance

TABLE II Composition of electropolishing solution for SEM specimens

Chemical	Composition (vol %)
Perchloric acid	22
Glacial acetic acid	78

TABLE III Composition of jet-polishing solution for TEM foils

Chemical	Composition (vol %)
Nitric acid	23
Methanol	77

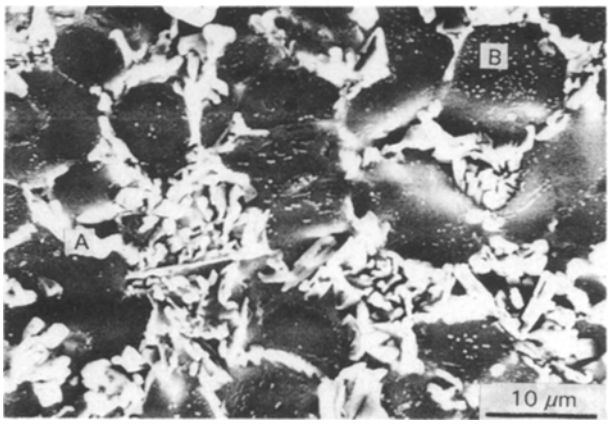

Figure 2 Primary and secondary silicon-rich particles in an aluminium-rich matrix of the as-cast material.

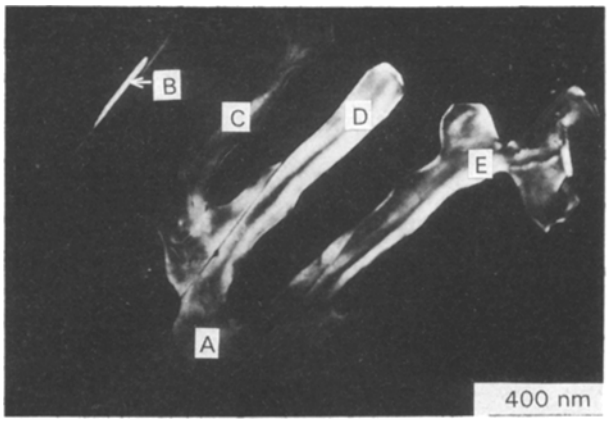

Figure 3 Dark-field image of a fibrous secondary silicon-rich particle in the as-cast material.

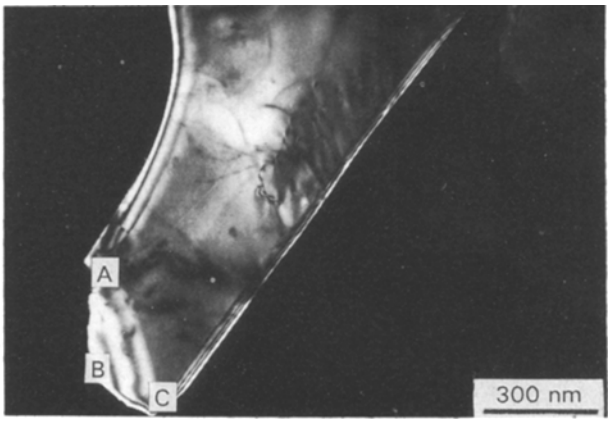

Figure 4 Dark-field image of a faceted plate-like secondary silicon-rich particle in the as-cast material.

this combination is spherical. This is because if the interfacial energy is isotropic, a sphere has the minimum surface area to volume ratio and hence minimum energy.

It is worth pointing out that there were very few fibrous particles in the as-cast material. Other secondary silicon-rich particles in the as-cast material had a plate-like morphology as shown in Fig. 4. The existence of plate-like secondary silicon-rich particles indicates that the interfacial energy is anisotropic. The faceted nature of the secondary silicon-rich particles is apparent; broad facets such as AB and BC exist on the habit plane. These facets are present on the secondary silicon-rich particle in order to minimize the interfacial energy required during nucleation. After the nucleation of these particles, growth commences. A $\langle 1\,1\,2 \rangle$ preferred growth direction has been observed in some silicon particles [15]. Note the irregular geometry of this plate-like secondary silicon-rich particle. A regular plate-shaped morphology that would normally be expected is shown in Fig. 5. Such a particle would have a habit plane (e.g. ABCD) bounded by narrower surfaces (e.g. CDEF). Needle-like particles (arrowed in Fig. 6) were also present in the as-cast material although at very low number densities. These were iron-containing particles which are $Al_{12}Fe_3Si$ and $(FeAl_6)Si$.

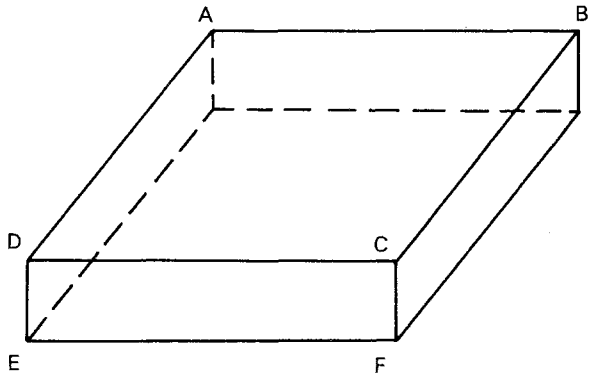

Figure 5 Geometry of a particle with a regular plate-shaped morphology.

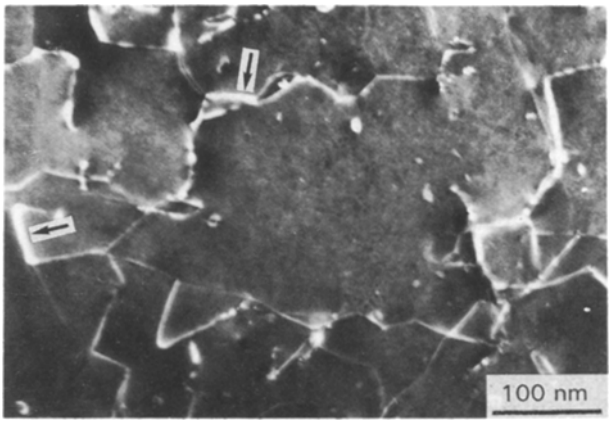

Figure 6 Weak-beam image of needle-like iron-containing particles in the as-cast material.

3.2. HIPed materials

Plate-like secondary silicon-rich particles also existed in the HIPed materials as shown in Fig. 7. As in the as-cast material, this plate-like particle has facets such as AB and BC on its habit plane. In addition, this particle has also an irregular plate morphology. It is interesting to note that after HIPing, fibrous particles were absent from the casting. There is evidence that in microstructures with fibrous or rod-like particles, instability is induced when the material is exposed to elevated temperatures [16]. Two types of structural defect, branches and terminations, are present in this type of particle [17] as shown in Fig. 8a. At elevated temperatures, such as those encountered during HIPing, diffusion-induced structural defect migration occurs when terminations and branches migrate in opposite directions (arrowed in Fig. 8b), consequently causing instability in fibrous particles. During migration collisions of these structural defects may occur, leading to their annihilation as shown in Fig. 8c. Annihilation of structural defects can simultaneously be accompanied by a change in morphology from fibrous or rod-like to cylindrical as evident in the central section of Fig. 8c.

Rod-like secondary silicon-rich particles were also present in the HIPed materials as can be seen in Fig. 9; these may have developed from structural defect migration in particles like those in Fig. 3. After HIPing most of the secondary silicon-rich particles still had a

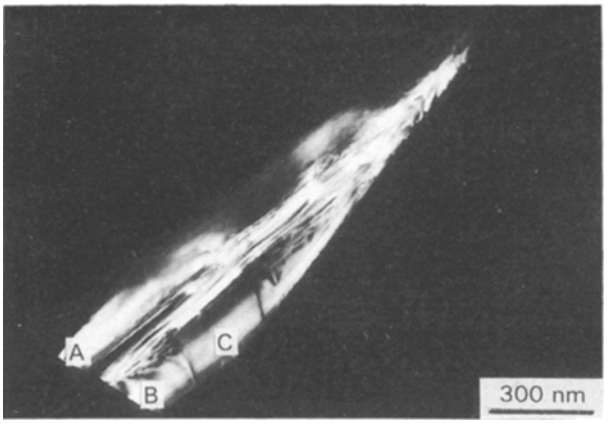

Figure 7 Dark-field image of a plate-like secondary silicon-rich particle after HIPing at 550 °C and 68.95 MPa for 120 min.

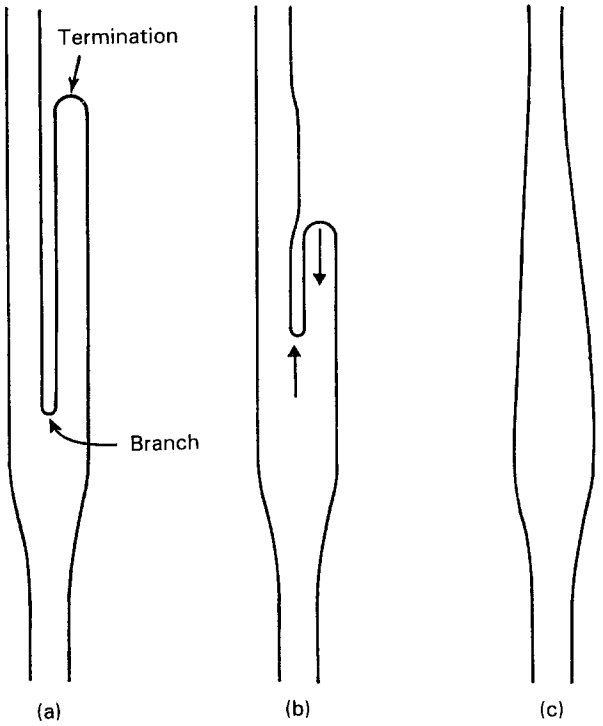

Figure 8(a–c) Scheme of annihilation of branch and termination in a rod-like or fibrous particle [17].

spherical morphology (Fig. 10). In addition, needle-like iron-containing particles (arrowed in Fig. 11) were also present in the HIPed materials. These are $Al_{12}Fe_3Si$ and $(FeAl_6)$ Si, which were also present in the as-cast material, in addition to new particles of $Al_9Fe_2Si_2$ which only precipitated during HIPing or heat treatment. From Fig. 11 it is apparent that these needle-like particles are confined to the aluminium-rich matrix in which a relatively high dislocation density is present.

3.3. Heat-treated materials

A few secondary silicon-rich particles with a plate-like morphology existed in the heat-treated materials as shown in Fig. 12. The number density of such particles was always very low. Most of the secondary silicon-rich particles, however, had a spherical morphology as can be seen in Fig. 13. Needle-like iron-containing particles existed in the heat-treated materials, though at very low number densities when the ageing time was 1 h. These iron-containing particles are $Al_{12}Fe_3Si$, $(FeAl_6)Si$ and $Al_9Fe_2Si_2$. The morphology of these particles did not change during heat treatment as shown in Fig. 14, in which needle-like particles (at A and B) are present in an aluminium-rich matrix con-

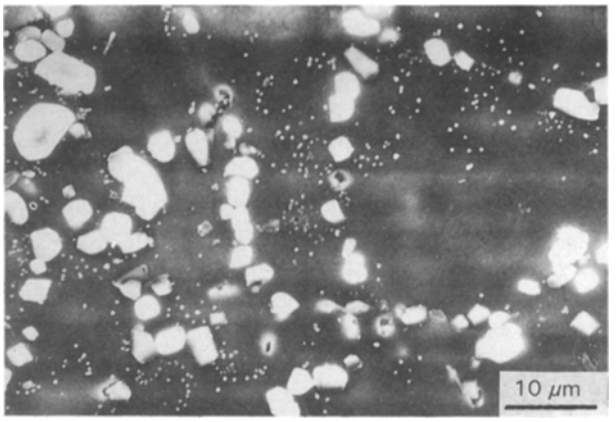

Figure 10 Spherical secondary silicon-rich particles after HIPing at 560 °C and 68.95 MPa for 120 min.

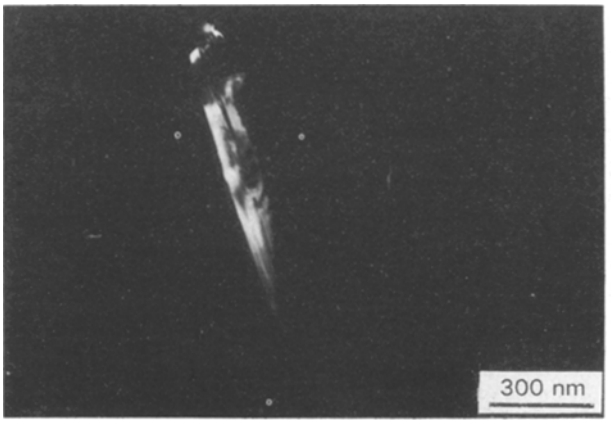

Figure 9 Dark-field image of a rod-like secondary silicon-rich particle after HIPing at 550 °C and 68.95 MPa for 120 min.

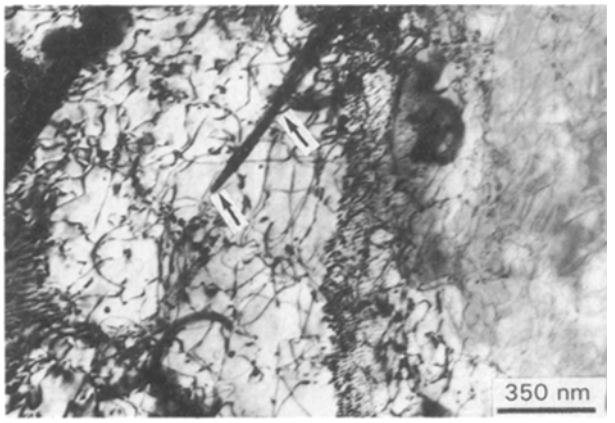

Figure 11 Bright-field image of iron-containing particles after HIPing at 550 °C and 68.95 MPa for 120 min.

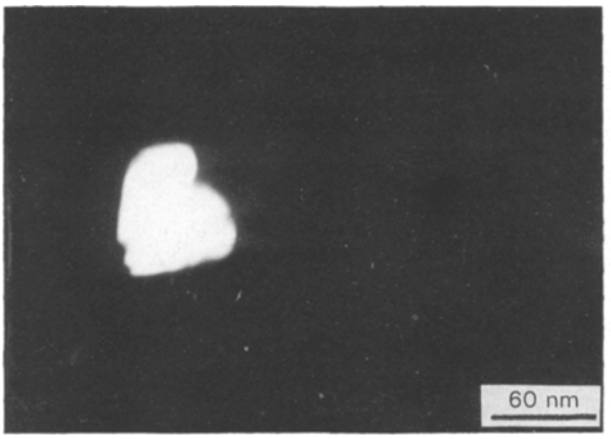

Figure 12 Dark-field image of a plate-like secondary silicon-rich particle after ageing for 48 h.

Figure 15 Weak-beam image of iron-containing particles after ageing for 48 h.

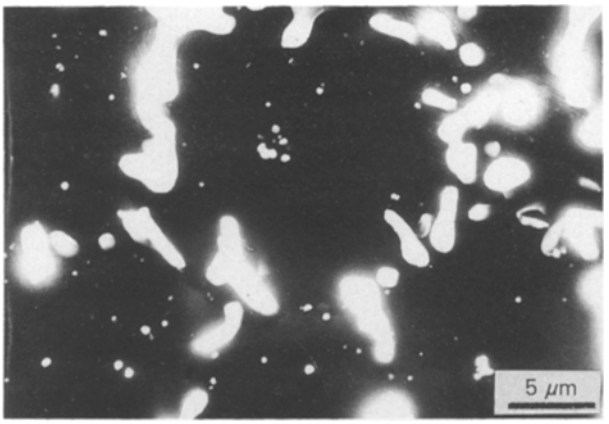

Figure 13 Spherical secondary silicon-rich particles after ageing for 1 h.

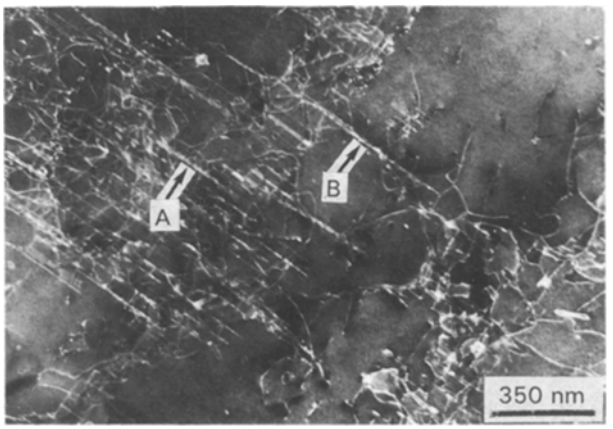

Figure 14 Weak-beam image of iron-containing particles after ageing for 1 h.

taining a very high dislocation density. It was of interest to investigate the effect of extended ageing time on the morphology of these particles. Consequently, some materials were aged for 48 h, rather than 1 h, after annealing and water-quenching. In these materials that had been aged for 48 h, parallel iron-containing particles (arrowed in Fig. 15) with a needle-like morphology existed. Since these particles are parallel to each other, this would suggest that they are rationally related to the aluminium-rich matrix. The morphology of these particles is, however, identical to that obtained after ageing for only 1 h. This implies that the morphology of iron-containing particles does not change with changing ageing time.

4. Conclusions

It has been established that the morphology of secondary silicon-rich particles in an as-cast Al–7.12 wt % Si alloy is plate-like, spherical or fibrous whereas that of the iron-containing particles is needle-like. In the HIPed or heat-treated materials, secondary silicon-rich particles are predominantly spherical. In a few instances, plate-like and rod-like secondary-rich particles were present in the HIPed materials although at very low number densities. In contrast, the iron-containing particles were insensitive to HIPing or heat treatment and precipitated with a needle-like morphology.

Acknowledgement

The author wishes to express gratitude to the Department of Materials Science and Engineering at The Pennsylvania State University for the provision of research facilities during this investigation.

References

1. J. W. MARTIN and R. D. DOHERTY, "Stability of Microstructure in Metallic Systems" (Cambridge University Press, 1976) p. 163.
2. S. MARICH, *Metall. Trans.* **1** (1970) 2953.
3. M. McLEAN, *Phil. Mag.* **27** (1973) 1253.
4. G. J. van GURP, *J. Appl. Phys.* **44** (1973) 2040.
5. G. C. WEATHERLY, *Acta Metall.* **19** (1971) 181.
6. J. K. LEE and H. I. AARONSON, *ibid.* **23** (1975) 799.
7. *Idem, ibid.* **23** (1975) 809.
8. W. C. JOHNSON, C. L. WHITE, P. E. MARTH, P. K. RUF, S. M. TUOMINEN, K. D. WADE, K. C. RUSSELL and H. I. AARONSON, *Metall. Trans. A* **6A** (1975) 911.
9. A. T. STEWART and J. W. MARTIN, *J. Inst. Metals* **98** (1970) 62.

10. R. WEST and H. FREDRIKSSON, *J. Mater. Sci.* **20** (1985) 1061.
11. H. FREDRIKSSON, M. HILLERT and N. LANGE, *J. Inst. Metals* **101** (1973) 285.
12. K. F. KOBAYASHI and L. M. HOGAN, *J. Mater. Sci.* **20** (1985) 1961.
13. D. K. CHATTERJEE and K. M. ENTWISTLE, *J. Inst. Metals* **101** (1973) 53.
14. J. YAN, L. CHUNZHI and Y. MINGGAO, *J. Mater. Sci.* **27** (1992) 197.
15. K. KOBAYASHI, P. H. SHINGU and R. OZAKI, *ibid.* **10** (1975) 290.
16. D. R. H. JONES, *Metal Sci.* **8** (1974) 37.
17. H. E. CLINE, *Acta Metall.* **19** (1971) 481.

Received 29 June 1992
and accepted 16 March 1993